Developmental Cell
Article

Role of RhoA-Specific Guanine Exchange Factors in Regulation of Endomitosis in Megakaryocytes

Yuan Gao,[1] Elenoe Smith,[3] Elmer Ker,[4] Phil Campbell,[4] Ee-chun Cheng,[3] Siying Zou,[1] Sharon Lin,[1] Lin Wang,[1] Stephanie Halene,[2] and Diane S. Krause[1,*]
[1]Department of Laboratory Medicine
[2]Department of Internal Medicine
Yale University, New Haven, CT 06520, USA
[3]Department of Cell Biology, Yale University, New Haven, CT 06905, USA
[4]Biomedical Engineering and Biological Sciences, Carnegie Mellon University, Pittsburgh, PA 15213, USA
*Correspondence: diane.krause@yale.edu
DOI 10.1016/j.devcel.2011.12.019

SUMMARY

Polyploidization can precede the development of aneuploidy in cancer. Polyploidization in megakaryocytes (Mks), in contrast, is a highly controlled developmental process critical for efficient platelet production via unknown mechanisms. Using primary cells, we demonstrate that the guanine exchange factors GEF-H1 and ECT2, which are often overexpressed in cancer and are essential for RhoA activation during cytokinesis, must be downregulated for Mk polyploidization. The first (2N–4N) endomitotic cycle requires GEF-H1 downregulation, whereas subsequent cycles (>4N) require ECT2 downregulation. Exogenous expression of both GEF-H1 and ECT2 prevents endomitosis, resulting in proliferation of 2N Mks. Furthermore, we have shown that the mechanism by which polyploidization is prevented in Mks lacking Mkl1, which is mutated in megakaryocytic leukemia, is via elevated GEF-H1 expression; shRNA-mediated GEF-H1 knockdown alone rescues this ploidy defect. These mechanistic insights enhance our understanding of normal versus malignant megakaryocytopoiesis, as well as aberrant mitosis in aneuploid cancers.

INTRODUCTION

Polyploidy resulting from cellular stress precedes aneuploidy, which can lead to tumors associated with transformation to malignancy and a poor prognosis (Nguyen and Ravid, 2006, 2010). In contrast, polyploidy of megakaryocytes (Mks), the hematopoietic cells that give rise to platelets, is a tightly controlled normal differentiation process. Diploid megakaryoblasts differentiated from hematopoietic stem cells undergo a progressive increase in ploidy (up to 128N) due to repeated DNA replication without cell division, a process termed endomitosis, resulting in large multilobulated, polyploid nuclei (Battinelli et al., 2007). Polyploidization is essential for efficient platelet production. In megakaryoblastic leukemia, low-ploidy megakaryoblasts predominate (Raslova et al., 2007).

Studies using time-lapse microscopy to observe endomitotic Mks suggest that the initial endomitotic cleavage event in which cells progress from 2N to 4N occurs due to failure at late cytokinesis with normal cleavage furrow ingression followed by furrow regression (Geddis et al., 2007; Papadantonakis et al., 2008; Lordier et al., 2008; Leysi-Derilou et al., 2010). These endomitotic Mks form an apparently intact midzone with normal localization of essential components including Survivin, Aurora B, INCENP, PRC1 (protein-regulating cytokinesis 1), MKLP1 and 2 (mitotic kinesin-like protein), MgcRacGAP, and microtubules (Geddis and Kaushansky, 2006; Lordier et al., 2008). During cytokinesis, RhoA signaling is required to establish the actomyosin ring at the cleavage furrow, generating the contraction force for completion of cytokinesis (Bement et al., 2005; Narumiya and Yasuda, 2006; Melendez et al., 2011). Activated RhoA and its effectors (ROCK, Citron, LIM, and mDia) are localized to the cleavage furrow (Madaule et al., 1998; Yasui et al., 1998; Kosako et al., 2000; Tolliday et al., 2002). Dominant-negative Citron and ROCK inhibitors prevent normal cytokinesis (Madaule et al., 1998; Kosako et al., 2000). In contrast to normal cytokinesis, the contractile ring of Mks undergoing endomitosis lacks nonmuscle myosin IIA and contains decreased levels of RhoA and actin at the 2N–4N transition; in higher ploidy cells, RhoA is not detectable at the cleavage furrow during anaphase (Geddis and Kaushansky, 2006; Lordier et al., 2008).

Rho family small GTPases (e.g., RhoA, Rac1, and Cdc42) are molecular switches that regulate many cellular processes, including actin cytoskeleton reorganization, microtubule dynamics, cell-cycle progression, and cytokinesis (Etienne-Manneville and Hall, 2002). Rho GTPase switching from the inactive GDP-bound state to the active GTP-bound state is facilitated by a group of proteins called Dbl family guanine nucleotide exchange factors (GEFs), which have a tandem Dbl homology (DH)-Pleckstrin homology (PH) domain, in which the DH domain contains GDP/GTP exchange activity (Rossman et al., 2005). GEFs are involved in RhoA localization and activation during different stages of cytokinesis. Upon breakdown of the nuclear envelope during mitosis, the GEF ECT2 (epithelial cell-transforming sequence 2) is dispersed from the nucleus to the cytoplasm, and recruited to the central spindle

by the central spindle complex (formed by MKlp1 and MgcRacGAP) during late anaphase for establishment of the cleavage furrow (Petronczki et al., 2007; Yüce et al., 2005). ECT2, required for cell-cycle progression, is an oncogene that resides on chromosome 3q26, a region frequently targeted for chromosomal alterations in human tumors and overexpressed in some primary human tumors (Fields and Justilien, 2010; Iyoda et al., 2010). RNA interference (RNAi) knockdown of ECT2 results in mitotic failure and binucleate cells due to lack of cleavage furrow ingression (Birkenfeld et al., 2007). There are multiple studies suggesting that ECT2 is important for RhoA localization and activation during cleavage furrow formation and ingression (Yüce et al., 2005; Nishimura and Yonemura, 2006; Yoshizaki et al., 2004), whereas some evidence suggested that ECT2 may not be directly responsible for RhoA activation during furrow ingression. Without ECT2, RhoA still gets activated but is mislocalized from the cleavage furrow (Chalamalasetty et al., 2006; Birkenfeld et al., 2007). An N-terminal fragment of ECT2 lacking the catalytic DH/PH domain can rescue the furrow ingression defect in ECT2 RNAi-treated cells (Chalamalasetty et al., 2006). Thus, ECT2 recruits RhoA to the cleavage furrow but may not directly catalyze its activation.

The microtubule-associated protein GEF-H1 plays a critical role in cytokinesis by activating RhoA at the cleavage furrow (Birkenfeld et al., 2007). Association with polymerized microtubules inactivates GEF-H1 (Krendel et al., 2002). A truncated form of GEF-H1 lacking its microtubule-binding ability was discovered in the monocytic leukemia cell line U937 and is able to induce tumor formation in nude mice (Brecht et al., 2005). Also, *GEF-H1* is transcriptionally activated by mutant p53, and its expression is strongly induced in mutant *p53* cell lines, leading to accelerated tumor cell proliferation (Mizuarai et al., 2006). During mitosis, GEF-H1 is first associated with the microtubule spindle, and later with the midbody (Birkenfeld et al., 2007). The same authors also show that GEF-H1 binding to microtubules is facilitated by phosphorylation at Ser^{885} and Ser^{959} by the mitotic kinases Aurora A/B and Cdk1, respectively. At the onset of cytokinesis, GEF-H1 is dephosphorylated and released from microtubules so that it can activate RhoA. In contrast to ECT2 RNAi, in which cytokinesis is blocked and there is no cleavage furrow formation, GEF-H1 knockdown causes a defect at a later stage of cytokinesis—the cleavage furrow is induced normally, but the furrow fails to close completely, resulting in binucleate cells (Birkenfeld et al., 2007).

Because of the importance of mitotic GEFs in RhoA localization and activation during cytokinesis, we hypothesized that decreased RhoA activation in Mk endomitosis may be caused by a decrease in mitotic GEFs. In the present work, we show that both GEF-H1 and ECT2 are downregulated at the mRNA and protein levels during Mk polyploidization. We show that MKL1-regulated GEF-H1 downregulation is required for endomitosis of 2N cells to become 4N, whereas ECT2 downregulation is required for polyploidization beyond the 4N stage. Together, these decreases in ECT2 and GEF-H1 are responsible for the decreased RhoA signaling that occurs in endomitosis, and downregulation of GEF-H1 represents one of the initiating events of endomitosis.

RESULTS

Establishment of In Vitro Models to Study Mk Endomitosis

We used primary murine Mks to study the involvement of Dbl family GEFs in Mk endomitosis. The first endomitotic event from 2N to 4N Mks occurs due to failure of cytokinesis at a late stage of cytokinesis with cleavage furrow regression. In contrast, there are different reports for when subsequent endomitotic events driving 4N to higher ploidy Mks interrupt the normal cytokinesis machinery. Some report significant cleavage furrow formation for higher ploidy Mks (Lordier et al., 2008; Leysi-Derilou et al., 2010), whereas others report little apparent cleavage furrow formation in high-ploidy endomitosis (Geddis et al., 2007; Papadantonakis et al., 2008). Therefore, we first examined how primary mouse Mks undergo endomitosis at different stages using Mks from GFP-tagged Histone 2B (H2B-GFP) transgenic mice visualized by time-lapse microscopy for changes in both chromatin and cell morphology during endomitosis. Mk progenitors (MkPs; Lin-Sca-$Kit^{+}CD41^{+}$) sorted from bone marrow (BM) were cultured in TPO-only differentiation medium (DM) to promote Mk polyploidization. MkP endomitotic events were recorded by time-lapse microscopy, and 2N, 4N, and higher ploidy MKs were distinguished based on division history as well as their cell size after mitosis or endomitosis, a method established previously (Levine et al., 1982; Leysi-Derilou et al., 2010; Tomer, 2004; Tomer et al., 1988). Of the 2N cells (24 events) whose DNA division events we observed, 80% of 2N DNA divisions resulted in endomitosis with clear cleavage furrow formation followed by regression and formation of 4N cells (Figure 1A; see Movie S1 available online), 7% of 2N cells underwent endomitosis without significant cleavage furrow ingression, and 13% of 2N cells underwent normal mitosis with complete cytokinesis. In contrast, for division of cells that started out with $\geq$4N DNA (37 events), 86% of divisions were endomitotic without noticeable cleavage furrow ingression (Figure 1B; Movie S2), and 14% were endomitotic with significant cleavage furrow ingression followed by regression. Our data confirm that there are two distinct phases of endomitosis in mouse primary Mks: for the 2N to 4N transition, the cleavage furrow forms but fails to complete cytokinesis; and for $\geq$4N endomitosis, there is usually, but not always, little to no cleavage furrow ingression.

RhoA Is Not Activated at the Cleavage Furrow during Endomitosis

RhoA activity is important for cleavage furrow ingression during cytokinesis. To understand the mechanisms underlying the failure to complete cytokinesis in 2N to 4N Mk endomitosis, we assayed localization of active RhoA during endomitosis using a FRET-based RhoA biosensor. The biphenotypic Mk-erythroid progenitor population as defined by Akashi et al. and refined (Lin-Sca-$Kit^{+}CD41^{-}CD150^{+}CD105^{-}$) and renamed "PreMegE" by Pronk et al. (Akashi et al., 2000; Pronk et al., 2007) was sorted from BM. To assess RhoA activation directly, a widely used single-molecule RhoA activation FRET probe (Birkenfeld et al., 2007; Pertz et al., 2006), pBabe-Puro-RhoA Biosensor, was transduced into primary mouse PreMegEs that were then cultured in growth medium (GM) (Figure 2A) or DM (Figure 2B), and the FRET efficiencies (FRET/CFP ratio) were determined

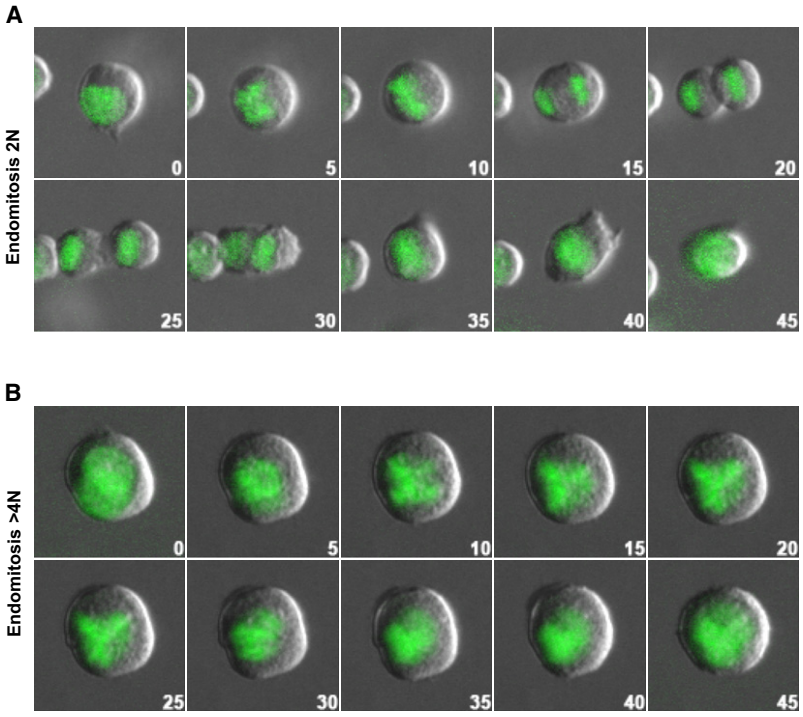

Figure 1. Endomitosis of MkPs Induced by TPO

(A) 2N to 4N Mk endomitosis shows cleavage furrow ingression with subsequent regression, resulting in one 4N cell.

(B) 4N to 8N Mk endomitosis showing no apparent cleavage furrow. The figures show overlays of DIC (gray) with green fluorescent H2B-GFP (green) images taken every 5 min. The time of each image relative to the first is indicated in each frame.

over time in cells undergoing anaphase using a Leica SP5-scanning microscope equipped with temperature and CO_2 control. Total RhoA localization was assessed by analysis of the CFP signal from the RhoA biosensor, which reflects the endogenous RhoA localization during mitosis as reported previously (Birkenfeld et al., 2007; Pertz et al., 2006). PreMegE cultured in GM with SCF, TPO, IL-3, and Flt-3 served as normal mitotic controls (Figure 2A). Under these conditions, 100% of 2N cells undergoing mitosis complete cytokinesis (data not shown). From early to late cytokinesis, the RhoA biosensor is enriched at the equatorial cortex (Figures 2Ai and 2Aiii) as previously reported (Yüce et al., 2005). When MkPs are cultured in DM, 80% of DNA divisions result in endomitosis, and during endomitotic anaphase and cytokinesis, RhoA is similarly present throughout the cytoplasm including at the equatorial region at early cytokinesis (Figures 2Bi and 2Biii), which is consistent with previous reports that RhoA localizes correctly during 2N endomitosis by immunofluorescence of fixed Mks (Geddis and Kaushansky, 2006; Lordier et al., 2008). To determine whether RhoA protein levels change during Mk differentiation, RhoA protein from different stages of Mk differentiation as well as in platelets was analyzed by western blotting. As shown in Figure S1, total RhoA protein was only slightly decreased (20%) during Mk differentiation, which is in agreement with the almost constant level of RhoA during Mk differentiation of $CD34^+$ human blood cells (Chang et al., 2007).

In PreMegE undergoing cytokinesis, there is a high FRET signal at the cleavage furrow (Figures 2Aii and 2Aiv) indicating high RhoA activity in this region, in agreement with published data on RhoA activation during cytokinesis in NIH 3T3 cells (Yoshizaki et al., 2003). However, in Mks undergoing endomitosis, there was no significant FRET signal in this region (Figures 2Bii and 2Biv), indicating lack of RhoA activation at the cleavage furrow, which provides direct evidence that during 2N to 4N endomitosis, there is a failure of RhoA activation at the cleavage furrow, even though RhoA is localized correctly to this region.

GEF-H1 and ECT2 Levels Decrease during Mk Polyploidization

To investigate the mechanisms underlying the failure of RhoA activation in Mks during endomitosis of 2N cells, and the absence of RhoA protein at the cleavage furrow region during endomitosis of higher ploidy cells, we assessed whether the mitosis-associated GEFs, ECT2 and GEF-H1, are differentially expressed during Mk differentiation. Wild-type (WT) PreMegEs and MkPs were cultured in DM, and RNA expression was assessed by quantitative RT-PCR over time. As shown in Figures 3A and 3B, MkPs had lower levels of both GEF-H1 and ECT2 mRNA compared with PreMegE. TPO treatment of PreMegE decreases GEF-H1 and ECT2 mRNA levels by 67% and 78%, respectively. GEF-H1 mRNA levels subsequently increased after prolonged TPO exposure when high-ploidy Mks were forming, whereas ECT2 mRNA levels remained low. GEF-H1 and ECT2 protein levels also decreased (Figure 3C) but with slightly different kinetics than the mRNA: GEF-H1 protein reached a nadir after 1 day of culture of PreMegE in TPO medium, and then began to increase; in contrast, ECT2 protein levels were significantly decreased after 2 days and then remained low.

GEF-H1 and ECT2 Levels during Endomitosis

ECT2 expression is induced by growth factors that promote cell-cycle entry, and cells in G0 have little ECT2 (Saito et al., 2003). However, it is unlikely that decreased GEF-H1 and ECT2 levels during TPO-induced Mk differentiation are caused by cell-cycle exit. First, TPO induces MkP cell cycling (Drayer et al., 2006). Second, the level of Anillin protein, an indicator of mitotic activity, which peaks in mitosis and decreases dramatically upon mitotic exit (Zhao and Fang, 2005), increased dramatically upon Mk TPO treatment (Figure S1), indicating increased cell cycling after TPO treatment. To directly confirm that Mks undergoing the cell cycle have decreased GEF-H1 and ECT2 levels, we examined GEF-H1 and ECT2 protein in endomitotic Mks by immunofluorescence. In mitotic control cells (PreMegEs in GM for 1 day), the microtubule spindle is normal, and GEF-H1 colocalizes with the microtubule spindle as reported previously (Birkenfeld et al., 2007) (Figures 4Ai–4Aiii). In contrast, in endomitotic MkPs cultured in DM for 1 day, the GEF-H1 protein level is low with little fluorescence

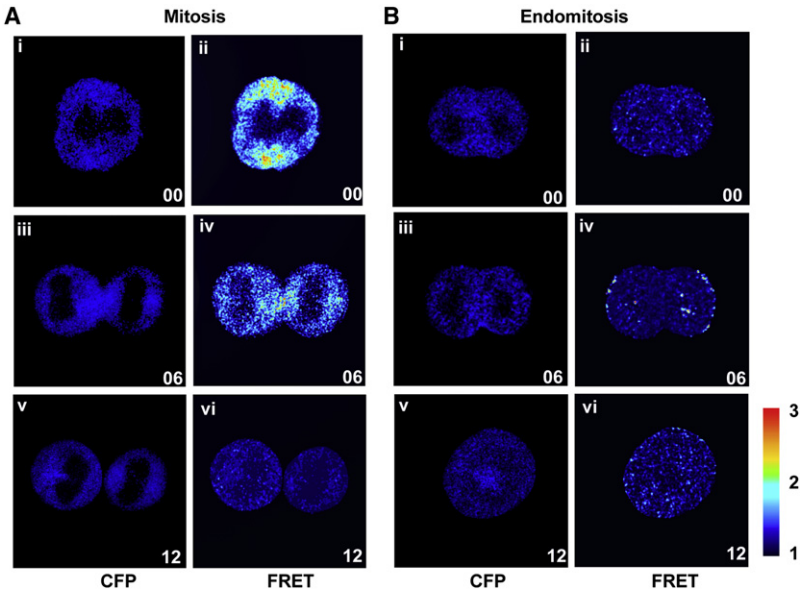

Figure 2. Active RhoA Is Absent from the Cleavage Furrow during the First Endomitotic Cleavage

Mouse primary PreMegE cells were transduced with the RhoA biosensor virus for 48 hr before switching to fresh GM (A) or DM (B). After 8 hr, the RhoA activation pattern throughout mitosis (A) or endomitosis (B) was assessed. The CFP channel indicates biosensor (and RhoA) localization (i, iii, and v). The RhoA activation pattern was ssessed by the RhoA biosensor's FRET/CFP ratio (FRET). The red color in FRET images indicates high RhoA activation (ii, iv, and vi). All images were processed identically. Elapsed time (minutes) with starting time set to zero (0) (8 hr post-TPO administration) is indicated in each picture. Images are representative of at least four similar observations for each condition.

signal detected above background (Figures 4Aiv and 4Avi). After 2 days in DM, in polyploid (>4N) cells undergoing anaphase, the spindle appeared normal, and GEF-H1 protein was again easily detected with localization to the microtubule spindle (Figures 4Avii–4Aix). The relative increase in GEF-H1 was consistent with the changes in protein levels detected by western blotting (Figure 3C). In PreMegE mitosis controls, ECT2 localized to the central spindle (Figures 4Bi–4Biii) as published previously (Tatsumoto et al., 1999; Yüce et al., 2005). During 2N to 4N endomitosis of MkPs, ECT2 was easily detected and localized to the central spindle (Figures 4Biv–4Bvi). The immunofluorescence signal between these two samples did not show any apparent differences (Figures 4Bi and 4Biv), although the ECT2 protein level in MkPs is about 30% lower than that of PreMegE by western blot (Figure 3C). In high-ploidy cells, ECT2 protein levels were very low (Figures 4Bvii–4Bix), which is in agreement with the western blot data (Figures 3C and S1). These data not only confirm that in endomitotic Mk cells, GEF-H1 and ECT2 levels decreased (albeit with different kinetics), but also suggest that during Mk differentiation, loss of GEF-H1 predominates in low-ploidy Mks, whereas loss of ECT2 occurs later and predominates in higher-ploidy endomitosis.

Ectopic Expression of GEF-H1 or ECT2 Causes Low-Ploidy Mks In Vitro

To test whether the decreases in GEF-H1 and/or ECT2 cause the sequential stages of endomitosis, we expressed exogenous GEF-H1 or ECT2 by retroviral transduction of PreMegE cells, which were then induced to differentiate with DM in which 80% of mitotic events are endomitotic. After 3 days in DM, the ploidy of GFP-positive (control vector versus ECT2 overexpression versus GEF-H1 overexpression) $CD41^+$ Mks was assessed by flow cytometry. Enforced expression of ECT2 or GEF-H1 did not affect the percentage of cells that were $CD41^+$ (Figure S2), suggesting that exogenous GEF-H1 or ECT2 does not affect PreMegE differentiation down the Mk lineage. Cells transduced with empty viral vector had a normal Mk ploidy distribution. Although enforced expression of either GEF-H1 or ECT2 resulted in significantly decreased mean ploidy (Figures 5A and 5B), the ploidy profiles were significantly different. GEF-H1 caused an increase in 2N cells, although Mks that became 4N were still able to become highly polyploid (Figure 5A, middle). In contrast, ECT2 expression led to accumulation at the 2N, 4N, and 8N stage with far fewer cells having >8N (Figure 5B, right). We believe that the 8N peak in cells overexpressing ECT2 represents the G2/M peak of cycling 4N cells. Expression of GEF-H1 and ECT2 was confirmed by western blot (Figure 5D). To evaluate whether enforced expression of GEF-H1 plus ECT2 completely prevents endomitosis, we transduced PreMegE cells with both GEF-H1 (with IRES-RFP) and ECT2 (with IRES-GFP) retroviruses. After 3 days in TPO, the ploidy of $CD41^+$ RFP+ and GFP+ (double-positive) cells was determined. Compared with cells only expressing GEF-H1 or ECT2, the cells expressing both have more 2N cells, and far fewer >4N cells (Figure 5C, far right, top). These data indicate that exogenous expression of GEF-H1 prevents the progression of cells from 2N to 4N in the first endomitotic event, whereas exogenous expression of ECT2 prevents the subsequent >4N endomitotic events to form highly polyploid Mks. Because RhoA acts downstream of ECT2 and GEF-H1, we next tested whether the dominant-negative RhoA mutant RhoA N19 can block the effect on Mk ploidy caused by enforced expression of ECT2 or GEF-H1 in Mks. As shown in Figure 5C (bottom), the ability to make high-ploidy Mks was restored in cells expressing both GEF-H1 and RhoA N19 or ECT2 and RhoA N19 compared with only expressing GEF-H1 or ECT2 (Figure 5C, top).

To assess whether downregulation of GEF-H1 plays a role in polyploidization of Mks in vivo, GEF-H1 transduced CD45.1 BM cells were transplanted into lethally irradiated WT CD45.2 mice. After 6 weeks, the ploidy of GFP-positive (control vector versus GEF-H1 transduced) Mks was assessed. In agreement with in vitro differentiation, ectopic expression of GEF-H1 resulted in more 2N Mks (27.8%) compared with empty vector (13.1%), leading to a decrease in the average ploidy (Figures 5E and 5F). However, as seen in vitro, those GEF-H1 transduced cells that did become 4N were able to undergo subsequent further polyploidization. These data demonstrate that enforced

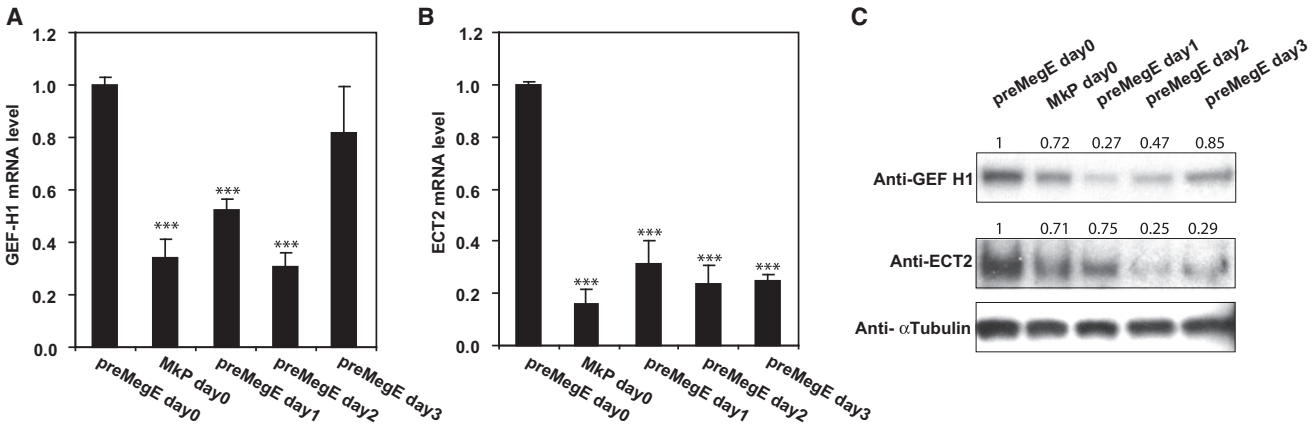

Figure 3. GEF-H1 and ECT2 Are Downregulated during Mk Differentiation

Data shown for freshly sorted (d0) PreMegE and MkP cells from WT mice, as well as PreMegEs cultured in DM for the time indicated.

(A) Relative levels of GEF-H1 mRNA are reduced during Mk differentiation. ***$p < 0.005$, versus value of PreMegE day 0.

(B) Relative levels of ECT2 mRNA were also decreased. ***$p < 0.005$, versus value of PreMegE day 0.

(C) The protein levels of GEF-H1 and ECT2 are reduced with different kinetics as shown by western blotting. Anti-α-tubulin was used as the loading control. Relative protein level of each sample after normalization to tubulin and setting PreMegE level as 1 are indicated above each band.

GEF-H1 expression decreases the likelihood of 2N to 4N endomitotic events in Mks in vivo.

Downregulation of GEF-H1 during Mk Differentiation Is Mediated by MKL1

Our lab previously demonstrated that knockout of the transcriptional cofactor Megakaryoblastic leukemia 1 gene (*Mkl1*) leads to reduced Mk ploidy in vivo (Cheng et al., 2009). To study whether the downregulation of GEF-H1 and/or ECT2 during Mk differentiation is Mkl1 dependent, we analyzed GEF-H1 and ECT2 mRNA levels during Mk differentiation of PreMegEs and MkPs from Mkl1$^{-/-}$ and WT mice. GEF-H1 levels in both PreMegEs and MkPs are more than 15 times higher in Mkl1$^{-/-}$ mice than in WT mice (Figure 6A). Unlike WT cells, there is little decrease of GEF-H1 mRNA in Mkl1$^{-/-}$ Mks differentiated in vitro. In contrast, ECT2 mRNA levels are the same in Mkl1$^{-/-}$ versus WT cells (Figure 6B).

We next assessed GEF-H1 protein expression and localization in Mkl1$^{-/-}$ versus WT PreMegEs cultured for 1 day in DM. GEF-H1 expression is much higher in Mkl1$^{-/-}$ Mks than WT, and it is localized to both the cell periphery and the microtubule spindle compared with predominant spindle localization in WT cells during normal mitosis (Figure 6C). No obvious differences between WT and Mkl1$^{-/-}$ cells were found in ECT2 detection or localization (data not shown). As expected with higher GEF-H1 levels in Mkl1$^{-/-}$ PreMegEs and Mks, GTP-bound active RhoA levels in PreMegEs with or without 24 hr exposure to TPO are higher than WT (Figure S3). However, the RhoA activity in Mkl1$^{-/-}$ cells is able to decrease after 1 day in TPO, similar to WT cells (Figure S3). To further confirm that GEF-H1 downregulation is MKL1 dependent, we assessed the GEF-H1 mRNA levels in nonhematopoietic 293FT cells transfected with control vector, WT, constitutively active, or dominant-negative MKL1 constructs. WT MKL1 slightly decreased GEF-H1, constitutively active MKL1 further decreased GEF-H1 levels, and dominant-negative MKL1 actually increased GEF-H1 levels (Figures 6D and 6E). MKL1 is part of the t(1;22)(p13;q13) chromosomal translocation, associated with acute megakaryoblastic leukemia (Mercher et al., 2001; Ma et al., 2001). To test whether GEF-H1 is dysregulated in acute megakaryoblastic leukemia containing the MKL1 translocation, we analyzed the levels of GEF-H1 and ECT2 in 6133 cells, a megakaryoblastic leukemia cell line derived from a transgenic mouse in which MKL1 was knocked in downstream of exon 1 of RBM15 to allow expression of the RBM15-MKL1 fusion product (Mercher et al., 2009), compared with WT PreMegEs. As shown (Figure 6F), 6133 cells express elevated GEF-H1 and ECT2 compared to normal MkP PreMegEs. In summary, GEF-H1 is downregulated by MKL1 during Mk differentiation, whereas the ECT2 decrease is MKL1 independent, and acute megakaryoblastic leukemia cells have increased GEF-H1 expression.

Knockdown of GEF-H1 Rescues the Ploidy Defect in Mkl1$^{-/-}$ Mks

In order to test whether downregulation of GEF-H1 alone can restore polyploidization in Mkl1$^{-/-}$ Mks, we decreased GEF-H1 by shRNA in WT and Mkl1$^{-/-}$ PreMegEs, that were then differentiated in DM. As expected, GEF-H1 shRNA had no effect on WT Mk ploidy compared with a control shRNA targeting luciferase (Figure 7A). Mks differentiated from Mkl1$^{-/-}$ cells transduced with control shRNA had lower ploidy than WT cells (Figure 7A). However, transduction of Mkl1$^{-/-}$ Mks with GEF-H1 shRNA led to much higher ploidy (Figure 7A, far right). The average ploidy for each condition (Figure 7B) demonstrates that shRNA against GEF-H1 restores the ploidy level of Mkl1$^{-/-}$ cells to that of WT cells. The GEF-H1 shRNA construct was validated in mouse NIH 3T3 cells, in which there was approximately 70% knockdown (Figure 7C).

DISCUSSION

Our data confirm that there are two distinct stages of Mk endomitosis. For the 2N to 4N transition, cleavage furrow ingression

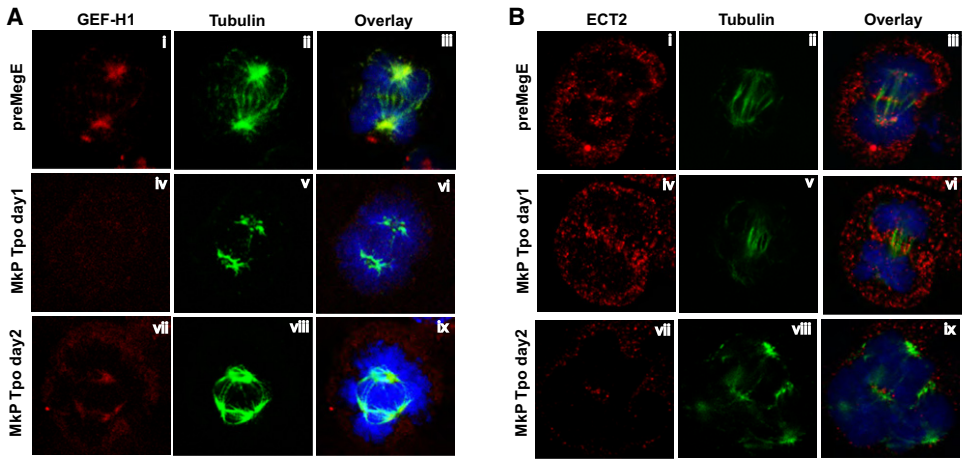

Figure 4. GEF-H1 and ECT2 Are Reduced in Endomitotic Mks

(A) Cells were stained with anti-GEF-H1 (red), anti-α-tubulin (green), and DAPI. Examples of normal mitosis (i–iii, PreMegEs cultured in GM), 2N to 4N endomitosis (iv–vi), and ≥4N endomitosis (vii–ix) are shown. GEF-H1 protein level is reduced at the 2N to 4N stage of endomitosis and increases at later stages (2 days) of endomitosis.

(B) ECT2 protein, stained with anti-ECT2 antibody (red), is clearly detected in PreMegEs undergoing mitosis (i–iii), and at the 2N to 4N stage of endomitosis (iv–vi), but ECT2 levels are reduced at later stages (2 days) of endomitosis (vii–ix).

occurs followed by furrow regression, whereas in endomitosis associated with ≥4N cells, there is little cleavage furrow ingression. Our data provide evidence that RhoA activation is absent from the cleavage furrow during endomitotic cleavage, and that two mitotic GEFs, GEF-H1 and ECT2, are downregulated during Mk differentiation. Overexpression of GEF-H1 in differentiating Mks leads to more 2N Mks, but for those cells that do fail to complete cytokinesis, high levels of polyploidization are still achievable. In contrast, exogenous ECT2 inhibits 4N polyploid cells from undergoing endomitosis but does not affect proliferation of 2N and 4N cells. Enforced overexpression of both GEF-H1 and ECT2 completely prevents polyploidization of primary Mks.

We conclude that decrease of GEF-H1 during megakaryocytopoiesis is mediated by the transcriptional cofactor MKL1, based on the markedly elevated GEF-H1 expression in Mkl1$^{-/-}$ Mks, and the downregulation of GEF-H1 in 293FT cells overexpressing constitutively active MKL1. The block of polyploidization in Mkl1$^{-/-}$ Mks can be restored by shRNA-mediated downregulation of GEF-H1, further confirming that GEF-H1 is downstream of MKL1.

Using primary murine PreMegEs and MkPs differentiated in vitro down the Mk lineage with TPO, we observed late cytokinesis defects in the first round of endomitosis, whereas for later rounds of endomitosis (≥4N), the majority of endomitosis occurred without apparent cleavage furrow ingression. These data differ from reports on endomitosis of human CD34+-derived Mks, especially cord blood CD34+, in which only about 30% of 2N cells undergo endomitosis, and the majority of high-ploidy cells showed significant furrow ingression, and some high-ploidy cells were able to complete cytokinesis and divide into two high-ploidy cells (Lordier et al., 2008; Leysi-Derilou et al., 2010). The low endomitosis ratio at the 2N stage of the human CD34+-derived Mks may be due to contamination with other cell types, and the majority of immunofluorescence images of those cells may represent normal mitotic divisions. Alternatively, there may be intrinsic differences between murine and human megakaryopoiesis, especially that of cord blood, in which Mk ploidy is lower than in adults, indicating fewer endomitotic cleavage events. Although the absence of cleavage furrow formation in high-ploidy endomitosis has been reported previously as being associated with a lack of accumulation of RhoA (Lordier et al., 2008; Geddis and Kaushansky, 2006), the mechanism of cytokinesis failure in the early rounds of endomitosis was previously unknown because RhoA was correctly localized to the cleavage furrow at the 2N stage. Here we show that this correctly localized RhoA is not activated in cells undergoing endomitosis with a FRET-based RhoA activity biosensor in live Mks.

We show that the mRNA and protein levels of two RhoA GEFs involved in cytokinesis are decreased with different kinetics during Mk differentiation: the reduction of GEF-H1 occurs at the 2N to 4N stage, whereas the significant reduction of ECT2 protein occurs at 4N and higher stages. Forced expression of GEF-H1 results in a higher percentage of Mks that are 2N, although high-ploidy Mks can still form, whereas forced expression of ECT2 results in accumulation of 2N to 8N Mks, and a lack of higher-ploidy Mks. Taken together, these data suggest that loss of GEF-H1 and ECT2 play distinct roles in Mk polyploidization: in low-ploidy cells, with correct ECT2 localization at the central spindle, RhoA is recruited to the equatorial region, but due to the lack of GEF-H1 protein, most of this RhoA is inactive. In high-ploidy cells, despite restored levels of GEF-H1, significantly decreased levels of ECT2 lead to failure of RhoA recruitment to the equatorial region. GEF-H1 levels decrease again in platelets (Figure S1). As we and others reported previously (Halene et al., 2010; Patel et al., 2005), the extensive microtubule network and actin cytoskeleton are essential for Mk maturation, platelet formation, and function. It is thus possible that the reappearance of GEF-H1, a unique

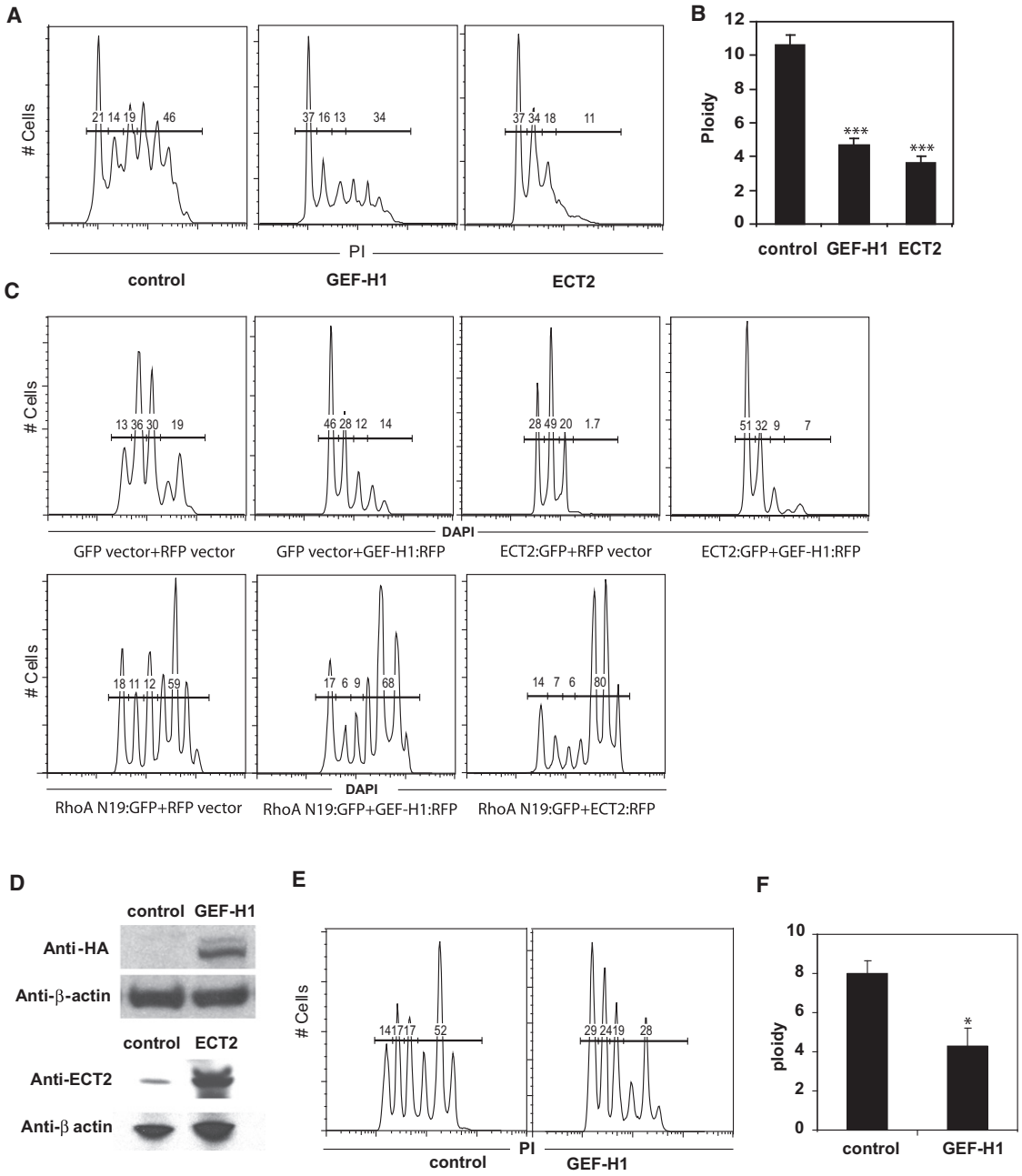

Figure 5. Differential Effects of Overexpressing GEF-H1 or ECT2 on Polyploidization of Mks

(A–C) PreMegE cells in GM were transduced with retroviral vectors (control and expressing individual GEFs) and cultured for 2 days, then transferred to DM for 3 days before the ploidy of each sample was assessed. (A) Shown is the effect of overexpressing control (GFP) virus, GEF-H1, or ECT2 encoding virus. Ploidy of GFP+ cells in each condition is shown. The percentages of Mks in 2N, 4N, and ≥8N ploidy are indicated. (B) The average ploidy of Mk expressing GFP only (control), GEF-H1, or ECT2 is compared. ***$p < 0.005$, versus control. (C) In this experiment, cells were transduced with two retroviral vectors (one encoding RFP and the other GFP). Controls received vectors encoding only RFP and GFP. GEF-H1 (top, second panel) received GFP control plus GEF-H1-IRES-RFP vectors, ECT2 (top, third panel) received ECT2-IRES-GFP plus control RFP vectors, the fourth panel (top) shows cells transduced with ECT2-IRES-GFP plus GEF-H1-IRES-RFP. Samples in lower panel were transduced with RhoAN19-IRES-GFP together with RFP control (left), GEF-H1-IRES-RFP (middle), or ECT2-IRES-RFP (right). Ploidy is shown for GFP+RFP+ (double-positive) cells.

(D) Western blot of HEL cells transduced with the indicated virus validates expression vectors.

(E) Overexpression of GEF-H1 also decreases polyploidization of Mks in vivo. CD45.1 BM cells were transduced with control (GFP only) or GEF-H1-IRES-GFP virus, and transplanted into lethally irradiated CD45.2 mice. After 6 weeks, the ploidy of GFP-positive Mks was analyzed. Representative ploidy profiles from GFP+ Mks expressing empty virus or GEF-H1 are shown.

(F) Average ploidy of GFP-positive Mks recovered 6 weeks posttransplant. *$p < 0.05$, versus the value of control.

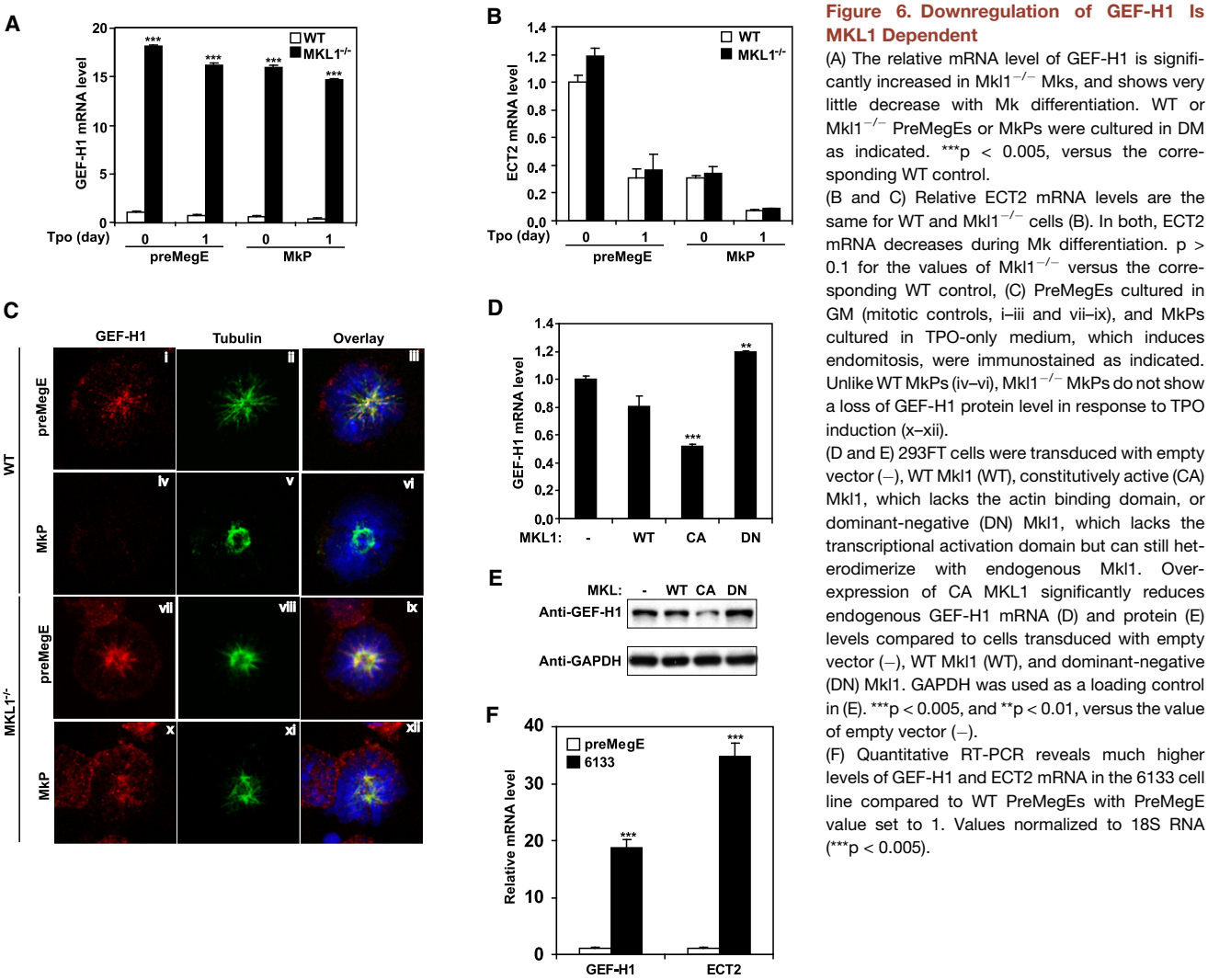

Figure 6. Downregulation of GEF-H1 Is MKL1 Dependent

(A) The relative mRNA level of GEF-H1 is significantly increased in Mkl1$^{-/-}$ Mks, and shows very little decrease with Mk differentiation. WT or Mkl1$^{-/-}$ PreMegEs or MkPs were cultured in DM as indicated. ***$p < 0.005$, versus the corresponding WT control.

(B and C) Relative ECT2 mRNA levels are the same for WT and Mkl1$^{-/-}$ cells (B). In both, ECT2 mRNA decreases during Mk differentiation. $p > 0.1$ for the values of Mkl1$^{-/-}$ versus the corresponding WT control, (C) PreMegEs cultured in GM (mitotic controls, i–iii and vii–ix), and MkPs cultured in TPO-only medium, which induces endomitosis, were immunostained as indicated. Unlike WT MkPs (iv–vi), Mkl1$^{-/-}$ MkPs do not show a loss of GEF-H1 protein level in response to TPO induction (x–xii).

(D and E) 293FT cells were transduced with empty vector (–), WT Mkl1 (WT), constitutively active (CA) Mkl1, which lacks the actin binding domain, or dominant-negative (DN) Mkl1, which lacks the transcriptional activation domain but can still heterodimerize with endogenous Mkl1. Overexpression of CA MKL1 significantly reduces endogenous GEF-H1 mRNA (D) and protein (E) levels compared to cells transduced with empty vector (–), WT Mkl1 (WT), and dominant-negative (DN) Mkl1. GAPDH was used as a loading control in (E). ***$p < 0.005$, and **$p < 0.01$, versus the value of empty vector (–).

(F) Quantitative RT-PCR reveals much higher levels of GEF-H1 and ECT2 mRNA in the 6133 cell line compared to WT PreMegEs with PreMegE value set to 1. Values normalized to 18S RNA (***$p < 0.005$).

microtubule-associated RhoA GEF, in higher-ploidy Mks may be essential for subsequent Mk maturation, but not for platelet function.

Our data from Mkl1$^{-/-}$ mice and overexpression of constitutively active (nuclear) MKL1 in 293FT cells suggest that MKL1 downregulates GEF-H1 mRNA, but not ECT2. MKL1 is a transcriptional cofactor for SRF. MKL1 is upregulated and required for Mk maturation and the formation of highly polyploid Mks (Cheng et al., 2009). There is a confirmed SRF binding site close to the GEF-H1 promoter region (Cooper et al., 2007). The mechanism by which MKL1 causes reduction of GEF-H1 during Mk differentiation requires further study.

Acute megakaryoblastic leukemia is characterized by a high percentage of immature, low-ploidy megakaryoblasts. We showed that GEF-H1 and ECT2 levels are dramatically increased in a megakaryoblastic leukemia cell line derived from a mouse AMKL model in which the t(1;22) fusion protein is encoded from the endogenous murine RBM15 locus. How and whether the RBM15-MKL1 fusion protein regulates GEF-H1 and/or ECT2 expression remains to be shown. One possibility is that RBM15-MKL1 inhibits MKL1 activity, but this would not explain the increase in ECT2 levels. Future studies will need to explore the levels of GEF-H1 and ECT2 in AMKL patient samples, and whether targeting of either of these GEFs could be used to promote Mk polyploidy and maturation.

Furthermore, these mechanistic insights into the normal polyploidization process of Mk differentiation have important implications for aneuploid cells, and their malignant transformation. In normal Mks, although there are high levels of cyclin E (Eliades et al., 2010) and D (Muntean et al., 2007) activity, which are required to overcome the cell-cycle checkpoints in high-ploidy cells undergoing endomitosis, proliferation is controlled due to the lack of GEF-H1 and ECT2, which promotes polyploidy and stops expansion. In contrast, abnormal polyploid cells formed under stress conditions, with highly active GEF-H1 and ECT2, can divide, expand, and transform to malignant aneuploid cells. Therefore, GEF-H1 and ECT2 are potential therapeutic targets for cancer cell proliferation and expansion.

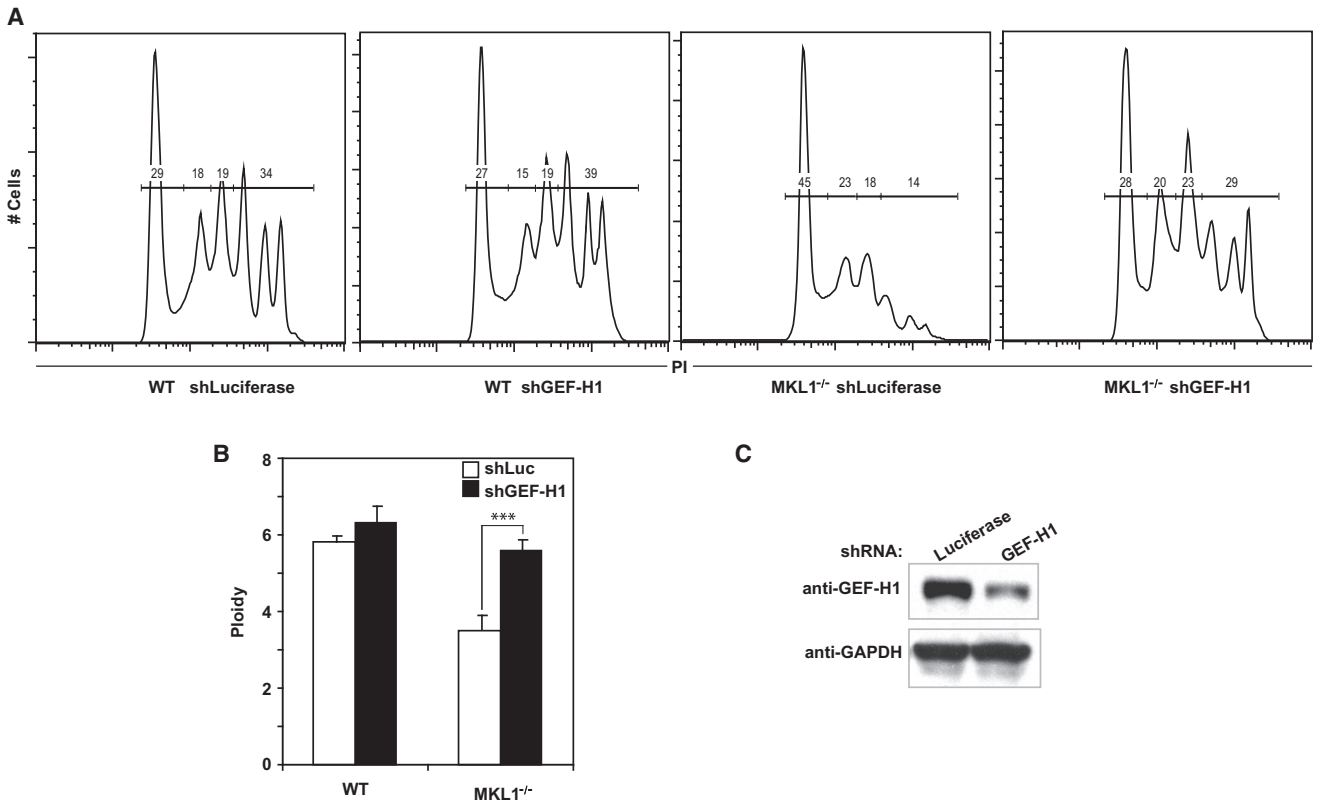

Figure 7. Knockdown of GEF-H1 Restores Polyploidy in Mkl1$^{-/-}$ Mks In Vitro

(A) WT or Mkl1$^{-/-}$ PreMegEs were transduced with retrovirus encoding either shRNA-targeting luciferase or GEF-H1, as indicated. After TPO induced differentiation, ploidy was assessed. A representative ploidy plot for each condition is shown. The percentages of Mks in 2N, 4N, 8N, and ≥16N ploidy are indicated.

(B) Average ploidy of these samples (***$p < 0.005$).

(C) Validation of shRNA-mediated knockdown of GEF-H1 protein in NIH 3T3 cells transduced with the indicated constructs. GFP-positive shRNA-expressing cells were sorted, and analyzed by western blot. GAPDH was used as the loading control.

EXPERIMENTAL PROCEDURES

Cell Sorting

All mouse procedures were performed according to Yale University Animal Care and Use Committee-approved protocols and complied with federal laws. Murine BM cells were obtained by crushing hips, femurs, and tibias in cold PBS with 1% FBS. After lineage depletion with the BD IMag Mouse Hematopoietic Progenitor (Stem) Cell Enrichment kit (BD Biosciences, San Jose, CA, USA), the remaining cells were stained with FITC anti-CD41, PE anti-lineage markers, PE-Cy5 anti-CD150, PE-Cy7 anti-CD105, Alexa 647 anti-Sca1, and APC-Hy7 anti-CD117 antibodies (eBioscience, San Diego, CA, USA; BioLegend, San Diego, CA, USA). The PreMegE population, defined as the Lin$^-$Sca$^-$Kit$^+$CD41$^-$CD105$^-$CD150$^+$, and MkP population, defined as Lin$^-$Sca$^-$Kit$^+$CD41$^+$, were separated using a FACSAria sorter. For sorting MkPs from H2B-GFP transgenic mice (Jackson Laboratory, Bar Harbor, ME, USA), eFluoro-450 labeled anti-CD41 antibody (eBioscience) was used.

Cell Culture, Mk Differentiation, and Western Blotting

For expansion, sorted PreMegEs were cultured at 1 × 10^6 cells/ml in GM containing StemSpan (StemCell Technologies, Vancouver, Canada) supplemented with 30% BIT9500 (StemCell Technologies), 100 ng/ml murine SCF, 50 ng/ml murine Flt3-L, 10 ng/ml murine IL-3 (all purchased from PeproTech, Rocky Hill, NJ, USA), 50 ng/ml murine TPO (from ConnStem, Cheshire, CT, USA), and penicillin/streptomycin. For differentiation, PreMegEs and MkPs were cultured in DM similar to the GM but with only a single cytokine, 20 ng/ml murine TPO. A total of 6,133 cells, a gift from Thomas Mercher (Villejuif, France), were grown as described (Mercher et al., 2009). For western blotting, about 1 × 10^5 cells per sample were washed with cold PBS, lysed in RIPA buffer for 15 min, and centrifuged at 18,000 × *g* for 15 min. Platelet lysate was prepared as described (Halene et al., 2010), and 20 μg of lysate per sample was analyzed by western blot with mouse anti-α-tubulin antibody (1:2,000; Sigma-Aldrich), rabbit anti-GEF-H1 antibody (1:1,000; Upstate), and rabbit anti-ECT2 antibody (1:500; Santa Cruz Biotechnology), and the corresponding secondary antibody. The density of protein bands was analyzed with ImageJ.

Time-Lapse Video Microscopy

Primary murine MkPs from H2B-GFP transgenic mice were sorted and cultured in 35 mm glass-bottom dishes (MatTeK, Ashland, MA, USA) in DM. To maintain nonadherent cells within the field of view for time-lapse microscopy, 1% methylcellulose was added to increase the viscosity. Live-cell imaging was performed using a VivaView system (Olympus; Japan) with a 20× objective. DIC and green fluorescence images were taken every 5 min for 2 days with an Orca-R2 camera (Hamamatsu, Japan). Imaging data were analyzed, compiled, and exported into QuickTime video with MetaMorph for VivaView software.

Immunofluorescent Staining and Confocal Analysis

PreMegE and MkP cells cultured as indicated were cytospun onto glass slides, fixed with 3.7% formaldehyde for 15 min, and permeabilized with 0.1% Triton X-100 (Sigma-Aldrich) for 15 min. After blocking (PBS plus 3% BSA), slides were incubated with mouse anti-α-tubulin plus rabbit anti-GEF-H1 antibody (1:200; Upstate) or rabbit anti-ECT2 antibody (1:100; Santa Cruz Biotechnology). Bound antibody was detected using Alexa 488-labeled

donkey anti-mouse secondary antibody and Alexa 555 donkey anti-rabbit secondary antibody, or Alexa 488-labeled anti-rabbit secondary antibody and Alexa 555 anti-mouse secondary antibody (Invitrogen). Fluorescent images were obtained on a Leica SP5 confocal microscope (Leica Microsystems, Wetzlar, Germany).

Plasmids, Virus Production, and PreMegE Transduction

Details regarding plasmids can be found in the Supplemental Experimental Procedures. For retrovirus production, in a T-175 flask, 90% confluent HEK293 cells constitutively expressing Gag/Pol were transfected with 40 μg pBabe-Puro-RhoA Biosensor, MigR1 empty vector control, MigR1-GEF-H1, MigR1-ECT2, or Mieg3 RhoA N19 and 14 μg of VSVG packaging plasmid by Lipofectamine 2000 (Invitrogen) per manufacturer's instructions. Supernatant collected at 48 and 72 hr was combined, spun at 3,700 × *g* through Amicon filters (Millipore, Billerica, MA, USA) to concentrate the virus to approximately 1×10^8 per ml, and aliquots were stored at −80°C. Freshly sorted 5×10^4 PreMegE cells in GM were infected with indicated viruses in the presence of polybrene (8 μg/ml) by spinfection at 900 × *g* for 1 hr at 30°C. After 2 days in GM, some cells were switched to DM for 8 hr before FRET analysis or another 3 days for ploidy analysis.

FRET Analysis of RhoA Activation in Endomitotic Cells

RhoA activity during endomitosis was visualized using a widely used RhoA biosensor FRET probe (Pertz et al., 2006). Two days after viral transduction, DNA of live PreMegE cells was stained with Hoechst red 33342 for 15 min, then the cells were washed and placed in DM or GM in a 35 mm glass-bottom dish. After 8 hr, dividing cells in prometaphase expressing the RhoA biosensor were identified by YFP-fluorescence and chromosome morphology by UV excitation on a Leica SP5 confocal microscope equipped with temperature and CO_2 control. CFP, FRET, YFP, and DIC images were acquired using a 63× NA 1.4 objective. The fluorescence emission resulting from excitation with 458 (for CFP and FRET) and 514 (for YFP) nm laser lines from an argon laser through an acousto-optical filter was detected with a prism spectrophotometer detection system, at a 490–500 nm spectral band width setting for CFP and a 520–590 nm spectral band width setting for FRET and YFP. Image analysis was performed using ImageJ essentially as described by Hodgson et al. (2010). Briefly, after shading correction and background subtraction, each CFP and the FRET image was multiplied with a binary threshold-based mask to eliminate noise outside of the cell. Then, the FRET ratio image was generated by dividing the raw FRET image with the CFP image.

Quantitative RT-PCR

Total RNA from 5×10^4 cells was isolated using the RNAqueous-Micro Kit (Applied Biosystems, Foster City, CA, USA), and treated with RNase-free DNase I. First-strand cDNA was produced with SuperScript II Reverse Transcriptase (Invitrogen) and random primers (Invitrogen) with 20 ng RNA from each sample. Gene expression levels were quantified on an iCycler iQ RT machine (Bio-Rad, Hercules, CA, USA) with 2 μl of cDNA product from each sample using TaqMan probes (Applied Biosystems) as follows: murine GEF-H1: Mm00434757_m1; murine ECT2: Mm01289559_g1; and Eukaryotic18S rRNA: Hs99999901_s1. Relative gene levels were calculated from standard curves and normalized to 18 s levels.

Flow Cytometric Analysis of DNA Content and Surface Markers

In vitro differentiated Mks were stained with APC-conjugated anti-CD41 antibody, then fixed and permeabilized using BD cytofix/cytoperm on ice for 30 min. After incubation with RNAase at 37°C for 30 min, nuclear DNA was stained with 1 g/ml propidium iodide and analyzed using a FACSCalibur cytometer (BD Biosciences) and FlowJo software (TreeStar, Ashland, OR, USA). In experiments using MigR1 RFP vectors, the nuclear DNA was stained with DAPI, and analyzed on a BD LSRII cytometer. To assay the Mk ploidy in transplanted mice, BM was collected, red cells lysed with PharmLyse (BD Biosciences), and ploidy analyzed as described above.

Murine BM Transplant

WT CD45.1 (B6.SJL-PtprcaPep3b/BoyJ mice) and CD45.2 (C57Bl6) mice were purchased from the Jackson Laboratory. After treatment with 150 mg/kg 5FU for 4 days, red cell-depleted BM from 4- to 6-week-old CD45.1 donor mice was transduced with empty vector or MigR1 GEF-H1 retrovirus by spinfection in StemSpan medium with 30% BIT9500, supplemented with 100 ng/ml SCF, 50 ng/ml TPO, 50 ng/ml Flt3 ligand, and 10 ng/ml IL-3. Lethally irradiated recipient C57Bl6/J mice were transplanted with 1 million cells 24 hr after transduction. Transplant efficiencies were monitored by detecting the CD45.1 ratio in the peripheral blood 4 weeks posttransplantation. GFP-positive Mk ploidy from recipient mice was analyzed 6 weeks posttransplant.

RNAi

The lentivirus pGIPZ vector containing shRNA-targeting GEF-H1 (RHS4430-101128431) was obtained from Open Biosystems. The mir30 shRNA GEF-H1 sequence was cut with restriction enzymes Hpa1 and Bsut1, and ligated into the CMV-YFP-shRNA retroviral vector (gift from D. Wu, Yale University) digested with Hpa1, and retrovirus produced as described above. CMV-YFP vector containing shRNA-targeting luciferase was used as a control. Sorted PreMegE cells from WT or $Mkl1^{-/-}$ mice (kind gift from Stephan Morris, Memphis, TN, USA) were transduced with the shRNA viruses, and incubated for 3 days in GM followed by 3 days in DM, and the ploidy of YFP-positive cells then assessed. To confirm the GEF-H1 shRNA efficiency, NIH 3T3 cells were also transduced. After 3 days, YFP cells were sorted, and GEF-H1 protein levels detected by western blot.

Statistical Analysis

Data are represented as mean ± SEM of at least three independent experiments. Statistical significance was calculated with Student's t test: $^*p < 0.05$, $^{**}p < 0.01$, $^{***}p < 0.005$.

SUPPLEMENTAL INFORMATION

Supplemental Information includes three figures, Supplemental Experimental Procedures, and two movies and can be found with this article online at doi:10.1016/j.devcel.2011.12.019.

ACKNOWLEDGMENTS

We thank Susannah Kassmer and Stephanie Donaldson for assistance with mice, Ping-Xia Zhang for expert technical assistance, and Emanuela Bruscia and Shangqin Guo for helpful discussions. We also thank Katherine Henderson for assistance with graphics. This work was supported by R01DK086267, the Yale Center of Excellence in Molecular Hematology (P30DK072442), the State of Connecticut Stem Cell Research Fund, and the Yale Cancer Center (P30CA016359). Y.G. designed and performed the study and wrote the manuscript. E.S. designed and created plasmids, performed experiments, modified manuscript, and provided intellectual input. E.K. and P.C. performed some time-lapse experiments. E.C. produced the stable HEL cell clones. S.Z. performed experiments and provided a figure. S.L. helped with mouse transplantation and other mouse work. L.W. provided assistance with plasmid and retroviral vectors. S.H. provided reagents and intellectual input. D.S.K. oversaw the studies and wrote the manuscript.

Received: April 22, 2011
Revised: November 22, 2011
Accepted: December 22, 2011
Published online: March 1, 2012

REFERENCES

Akashi, K., Traver, D., Miyamoto, T., and Weissman, I.L. (2000). A clonogenic common myeloid progenitor that gives rise to all myeloid lineages. Nature *404*, 193–197.

Battinelli, E.M., Hartwig, J.H., and Italiano, J.E., Jr. (2007). Delivering new insight into the biology of megakaryopoiesis and thrombopoiesis. Curr. Opin. Hematol. *14*, 419–426.

Bement, W.M., Benink, H.A., and von Dassow, G. (2005). A microtubule-dependent zone of active RhoA during cleavage plane specification. J. Cell Biol. *170*, 91–101.

Birkenfeld, J., Nalbant, P., Bohl, B.P., Pertz, O., Hahn, K.M., and Bokoch, G.M. (2007). GEF-H1 modulates localized RhoA activation during cytokinesis under the control of mitotic kinases. Dev. Cell *12*, 699–712.

Brecht, M., Steenvoorden, A.C., Collard, J.G., Luf, S., Erz, D., Bartram, C.R., and Janssen, J.W. (2005). Activation of gef-h1, a guanine nucleotide exchange factor for RhoA, by DNA transfection. Int. J. Cancer *113*, 533–540.

Chalamalasetty, R.B., Hümmer, S., Nigg, E.A., and Silljé, H.H. (2006). Influence of human Ect2 depletion and overexpression on cleavage furrow formation and abscission. J. Cell Sci. *119*, 3008–3019.

Chang, Y., Auradé, F., Larbret, F., Zhang, Y., Le Couedic, J.P., Momeux, L., Larghero, J., Bertoglio, J., Louache, F., Cramer, E., et al. (2007). Proplatelet formation is regulated by the Rho/ROCK pathway. Blood *109*, 4229–4236.

Cheng, E.C., Luo, Q., Bruscia, E.M., Renda, M.J., Troy, J.A., Massaro, S.A., Tuck, D., Schulz, V., Mane, S.M., Berliner, N., et al. (2009). Role for MKL1 in megakaryocytic maturation. Blood *113*, 2826–2834.

Cooper, S.J., Trinklein, N.D., Nguyen, L., and Myers, R.M. (2007). Serum response factor binding sites differ in three human cell types. Genome Res. *17*, 136–144.

Drayer, A.L., Olthof, S.G., and Vellenga, E. (2006). Mammalian target of rapamycin is required for thrombopoietin-induced proliferation of megakaryocyte progenitors. Stem Cells *24*, 105–114.

Eliades, A., Papadantonakis, N., and Ravid, K. (2010). New roles for cyclin E in megakaryocytic polyploidization. J. Biol. Chem. *285*, 18909–18917.

Etienne-Manneville, S., and Hall, A. (2002). Rho GTPases in cell biology. Nature *420*, 629–635.

Fields, A.P., and Justilien, V. (2010). The guanine nucleotide exchange factor (GEF) Ect2 is an oncogene in human cancer. Adv. Enzyme Regul. *50*, 190–200.

Geddis, A.E., and Kaushansky, K. (2006). Endomitotic megakaryocytes form a midzone in anaphase but have a deficiency in cleavage furrow formation. Cell Cycle *5*, 538–545.

Geddis, A.E., Fox, N.E., Tkachenko, E., and Kaushansky, K. (2007). Endomitotic megakaryocytes that form a bipolar spindle exhibit cleavage furrow ingression followed by furrow regression. Cell Cycle *6*, 455–460.

Halene, S., Gao, Y., Hahn, K., Massaro, S., Italiano, J.E., Jr., Schulz, V., Lin, S., Kupfer, G.M., and Krause, D.S. (2010). Serum response factor is an essential transcription factor in megakaryocytic maturation. Blood *116*, 1942–1950.

Hodgson, L., Shen, F., and Hahn, K. (2010). Biosensors for characterizing dynamics of Rho family GTPases in living cells. Curr. Protoc. Cell Biol., Chapter 14, 14.11.1–14.11.26.

Iyoda, M., Kasamatsu, A., Ishigami, T., Nakashima, D., Endo-Sakamoto, Y., Ogawara, K., Shiiba, M., Tanzawa, H., and Uzawa, K. (2010). Epithelial cell transforming sequence 2 in human oral cancer. PLoS ONE *5*, e14082.

Kosako, H., Yoshida, T., Matsumura, F., Ishizaki, T., Narumiya, S., and Inagaki, M. (2000). Rho-kinase/ROCK is involved in cytokinesis through the phosphorylation of myosin light chain and not ezrin/radixin/moesin proteins at the cleavage furrow. Oncogene *19*, 6059–6064.

Krendel, M., Zenke, F.T., and Bokoch, G.M. (2002). Nucleotide exchange factor GEF-H1 mediates cross-talk between microtubules and the actin cytoskeleton. Nat. Cell Biol. *4*, 294–301.

Levine, R.F., Hazzard, K.C., and Lamberg, J.D. (1982). The significance of megakaryocyte size. Blood *60*, 1122–1131.

Leysi-Derilou, Y., Robert, A., Duchesne, C., Garnier, A., Boyer, L., and Pineault, N. (2010). Polyploid megakaryocytes can complete cytokinesis. Cell Cycle *9*, 2589–2599.

Lordier, L., Jalil, A., Aurade, F., Larbret, F., Larghero, J., Debili, N., Vainchenker, W., and Chang, Y. (2008). Megakaryocyte endomitosis is a failure of late cytokinesis related to defects in the contractile ring and Rho/Rock signaling. Blood *112*, 3164–3174.

Ma, Z., Morris, S.W., Valentine, V., Li, M., Herbrick, J.A., Cui, X., Bouman, D., Li, Y., Mehta, P.K., Nizetic, D., et al. (2001). Fusion of two novel genes, RBM15 and MKL1, in the t(1;22)(p13;q13) of acute megakaryoblastic leukemia. Nat. Genet. *28*, 220–221.

Madaule, P., Eda, M., Watanabe, N., Fujisawa, K., Matsuoka, T., Bito, H., Ishizaki, T., and Narumiya, S. (1998). Role of citron kinase as a target of the small GTPase Rho in cytokinesis. Nature *394*, 491–494.

Melendez, J., Stengel, K., Zhou, X., Chauhan, B.K., Debidda, M., Andreassen, P., Lang, R.A., and Zheng, Y. (2011). RhoA GTPase is dispensable for actomyosin regulation but is essential for mitosis in primary mouse embryonic fibroblasts. J. Biol. Chem. *286*, 15132–15137.

Mercher, T., Coniat, M.B., Monni, R., Mauchauffé, M., Nguyen Khac, F., Gressin, L., Mugneret, F., Leblanc, T., Dastugue, N., Berger, R., and Bernard, O.A. (2001). Involvement of a human gene related to the Drosophila spen gene in the recurrent t(1;22) translocation of acute megakaryocytic leukemia. Proc. Natl. Acad. Sci. USA *98*, 5776–5779.

Mercher, T., Raffel, G.D., Moore, S.A., Cornejo, M.G., Baudry-Bluteau, D., Cagnard, N., Jesneck, J.L., Pikman, Y., Cullen, D., Williams, I.R., et al. (2009). The OTT-MAL fusion oncogene activates RBPJ-mediated transcription and induces acute megakaryoblastic leukemia in a knockin mouse model. J. Clin. Invest. *119*, 852–864.

Mizuarai, S., Yamanaka, K., and Kotani, H. (2006). Mutant p53 induces the GEF-H1 oncogene, a guanine nucleotide exchange factor-H1 for RhoA, resulting in accelerated cell proliferation in tumor cells. Cancer Res. *66*, 6319–6326.

Muntean, A.G., Pang, L., Poncz, M., Dowdy, S.F., Blobel, G.A., and Crispino, J.D. (2007). Cyclin D-Cdk4 is regulated by GATA-1 and required for megakaryocyte growth and polyploidization. Blood *109*, 5199–5207.

Narumiya, S., and Yasuda, S. (2006). Rho GTPases in animal cell mitosis. Curr. Opin. Cell Biol. *18*, 199–205.

Nguyen, H.G., and Ravid, K. (2006). Tetraploidy/aneuploidy and stem cells in cancer promotion: The role of chromosome passenger proteins. J. Cell. Physiol. *208*, 12–22.

Nguyen, H.G., and Ravid, K. (2010). Polyploidy: mechanisms and cancer promotion in hematopoietic and other cells. Adv. Exp. Med. Biol. *676*, 105–122.

Nishimura, Y., and Yonemura, S. (2006). Centralspindlin regulates ECT2 and RhoA accumulation at the equatorial cortex during cytokinesis. J. Cell Sci. *119*, 104–114.

Papadantonakis, N., Makitalo, M., McCrann, D.J., Liu, K., Nguyen, H.G., Martin, G., Patel-Hett, S., Italiano, J.E., and Ravid, K. (2008). Direct visualization of the endomitotic cell cycle in living megakaryocytes: differential patterns in low and high ploidy cells. Cell Cycle *7*, 2352–2356.

Patel, S.R., Richardson, J.L., Schulze, H., Kahle, E., Galjart, N., Drabek, K., Shivdasani, R.A., Hartwig, J.H., and Italiano, J.E., Jr. (2005). Differential roles of microtubule assembly and sliding in proplatelet formation by megakaryocytes. Blood *106*, 4076–4085.

Pertz, O., Hodgson, L., Klemke, R.L., and Hahn, K.M. (2006). Spatiotemporal dynamics of RhoA activity in migrating cells. Nature *440*, 1069–1072.

Petronczki, M., Glotzer, M., Kraut, N., and Peters, J.M. (2007). Polo-like kinase 1 triggers the initiation of cytokinesis in human cells by promoting recruitment of the RhoGEF Ect2 to the central spindle. Dev. Cell *12*, 713–725.

Pronk, C.J., Rossi, D.J., Månsson, R., Attema, J.L., Norddahl, G.L., Chan, C.K., Sigvardsson, M., Weissman, I.L., and Bryder, D. (2007). Elucidation of the phenotypic, functional, and molecular topography of a myeloerythroid progenitor cell hierarchy. Cell Stem Cell *1*, 428–442.

Raslova, H., Kauffmann, A., Sekkaï, D., Ripoche, H., Larbret, F., Robert, T., Le Roux, D.T., Kroemer, G., Debili, N., Dessen, P., et al. (2007). Interrelation between polyploidization and megakaryocyte differentiation: a gene profiling approach. Blood *109*, 3225–3234.

Rossman, K.L., Der, C.J., and Sondek, J. (2005). GEF means go: turning on RHO GTPases with guanine nucleotide-exchange factors. Nat. Rev. Mol. Cell Biol. *6*, 167–180.

Saito, S., Tatsumoto, T., Lorenzi, M.V., Chedid, M., Kapoor, V., Sakata, H., Rubin, J., and Miki, T. (2003). Rho exchange factor ECT2 is induced by growth factors and regulates cytokinesis through the N-terminal cell cycle regulator-related domains. J. Cell. Biochem. *90*, 819–836.

Tatsumoto, T., Xie, X., Blumenthal, R., Okamoto, I., and Miki, T. (1999). Human ECT2 is an exchange factor for Rho GTPases, phosphorylated in G2/M phases, and involved in cytokinesis. J. Cell Biol. *147*, 921–928.

Tolliday, N., VerPlank, L., and Li, R. (2002). Rho1 directs formin-mediated actin ring assembly during budding yeast cytokinesis. Curr. Biol. *12*, 1864–1870.

Tomer, A. (2004). Human marrow megakaryocyte differentiation: multiparameter correlative analysis identifies von Willebrand factor as a sensitive and distinctive marker for early (2N and 4N) megakaryocytes. Blood *104*, 2722–2727.

Tomer, A., Harker, L.A., and Burstein, S.A. (1988). Flow cytometric analysis of normal human megakaryocytes. Blood *71*, 1244–1252.

Yasui, Y., Amano, M., Nagata, K., Inagaki, N., Nakamura, H., Saya, H., Kaibuchi, K., and Inagaki, M. (1998). Roles of Rho-associated kinase in cytokinesis; mutations in Rho-associated kinase phosphorylation sites impair cytokinetic segregation of glial filaments. J. Cell Biol. *143*, 1249–1258.

Yoshizaki, H., Ohba, Y., Kurokawa, K., Itoh, R.E., Nakamura, T., Mochizuki, N., Nagashima, K., and Matsuda, M. (2003). Activity of Rho-family GTPases during cell division as visualized with FRET-based probes. J. Cell Biol. *162*, 223–232.

Yoshizaki, H., Ohba, Y., Parrini, M.C., Dulyaninova, N.G., Bresnick, A.R., Mochizuki, N., and Matsuda, M. (2004). Cell type-specific regulation of RhoA activity during cytokinesis. J. Biol. Chem. *279*, 44756–44762.

Yüce, O., Piekny, A., and Glotzer, M. (2005). An ECT2-centralspindlin complex regulates the localization and function of RhoA. J. Cell Biol. *170*, 571–582.

Zhao, W.M., and Fang, G. (2005). Anillin is a substrate of anaphase-promoting complex/cyclosome (APC/C) that controls spatial contractility of myosin during late cytokinesis. J. Biol. Chem. *280*, 33516–33524.